Available on CMS information server

CMS NOTE 2006/086

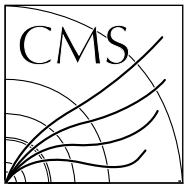

The Compact Muon Solenoid Experiment

CMS Note

Mailing address: CMS CERN, CH-1211 GENEVA 23, Switzerland

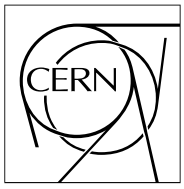

30 May 2006

Search for W-associated Production of Single Top Quarks in CMS

P. Yeh, K.F. Chen, Y.J. Lei, J. Schuemann, Y. Chao, J.-G. Shiu

National Taiwan University, Taipei, Taiwan

A. Giammanco

Université catholique de Louvain, Louvain-la-Neuve, Belgium

G. Petrucciani

SNS & INFN Pisa, Pisa, Italy

S. Blyth

National Central University, Chungli, Taiwan

Abstract

The production of single top quarks at the LHC provides a unique window onto the measurement of the Cabibbo-Kobayashi-Maskawa matrix element $|\mathrm{V_{tb}}|$ without assuming three generation unitarity. The W-associated production of single top is a challenging channel due to the large overlap in phase space with $\mathrm{t\bar{t}}$ production. A ratio method is developed to effectively reduce the systematic uncertainties in the presence of large $\mathrm{t\bar{t}}$ backgrounds. The expected uncertainties and significance for a 60 pb $\mathrm{pp} \rightarrow \mathrm{tW}$ production cross section with 10 fb^{-1} of CMS data are presented.

1 Introduction

The production of single top quarks through or with weak vector bosons is predicted to exist in the Standard Model. There are three major processes for single top quark production: t channel ($\mathrm{bq} \to \mathrm{tq}'$), s channel ($\bar{\mathrm{q}}\mathrm{q}' \to \mathrm{t}\bar{\mathrm{b}}$) and W-associated production ($\mathrm{bg} \to \mathrm{tW}^-$)[1)], which have been hailed as the next stage of precision top physics studies. The leading order Feynman diagrams of the single top productions are shown in figure 1.

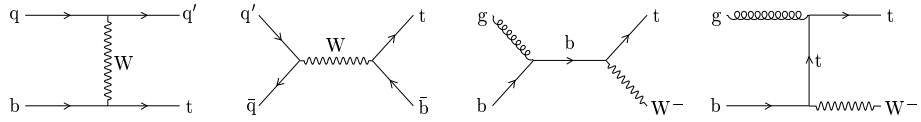

Figure 1: Leading order Feynman diagrams of the single top processes. From left to right: t channel, s channel and two diagrams for W-associated productions.

Single top processes have a unique place in the Standard Model: the production cross sections are directly proportional to the Cabibbo-Kobayashi-Maskawa (CKM) matrix element $|\mathrm{V_{tb}}|^2$. A measurement of the production cross section is a direct measurement of $|\mathrm{V_{tb}}|$ without assuming 3 generations or unitarity of the CMK matrix [1], while all previous measurements of $|\mathrm{V_{tb}}|$ have assumed 3 generations [2, 3]. An accurate and direct measurement of $|\mathrm{V_{tb}}|$ may put stringent constraints on the parameter space of the fourth generation of elementary particles, or even eradicate any arguments in favor of the existence of a fourth generation. On the other hand, if $|\mathrm{V_{tb}}|$ turns out to have a significant deviation from the three-generation unitarity assumption, it would make room for the existence of fourth generation quarks and leptons or a non-SM W-t-b coupling.

Searches for single top events are being carried out in the Tevatron right now. However the standard model cross sections are expected to be small at the Tevatron: σ(t channel) = 1.98 pb ($\pm$11%), σ(s channel) = 0.88 pb ($\pm$8%) and $\sigma(\mathrm{tW})$ = 0.14 pb ($\pm$15%) [4, 5]. With the current integrated luminosity of $\sim$ 1 fb^{-1} at the Tevatron, no significant observations have been claimed. The standard model cross sections are much larger at the Large Hadron Collider (LHC) due to the energies available and abundance of gluons: σ(t channel) = 247 pb ($\pm$5%), σ(s channel) = 10.7 pb ($\pm$10%) and $\sigma(\mathrm{tW})$ = 68 pb ($\pm$10%) [4, 5].

Most experimental and theoretical studies on single top processes have concentrated on the t channel due to its larger cross section and on the s channel due to its cleaner final state. The W-associated production of single top quarks, on the other hand, has gained attention only recently.

Experimentally, tW production is also important as it is a background to the $\mathrm{gg} \to \mathrm{H} \to \mathrm{W^+W^-}$ and $\mathrm{gb} \to \mathrm{tH^-}$ processes. It is impractical to claim discovery of the Higgs boson in these channels without an observation of the standard model tW process in advance with real data. Therefore tW production is a process that paves the way for new physics.

Theoretically, it is a complicated process to calculate due to the presence of next to leading order (NLO) diagrams like $\mathrm{gg} \to \mathrm{gb\bar{b}} \to \mathrm{tW^-\bar{b}}$. If the immediate decay products of the top quark are considered, this process has an identical initial state and final state with the $\mathrm{gg} \to \mathrm{t\bar{t}}$ process, namely $\mathrm{gg} \to \mathrm{W^+W^-b\bar{b}}$. Therefore there is an interference [5, 6, 7, 8]. Because the $\mathrm{t\bar{t}}$ production has a much larger cross section at the LHC ($\sim$830 pb in NLO calculations), it is not trivial, from the theoretical point of view, to handle the interference and extract a self-consistent treatment of tW production. A consistent Monte Carlo treatment of the tW process, the $\mathrm{t\bar{t}}$ process and parton distribution functions (PDF) together is necessary to avoid double counting.

Unlike the t and s channels, the rates of $\mathrm{bg} \to \mathrm{tW^-}$ and its charge conjugate process are the same at the LHC because the parton distribution functions for b and $\bar{\mathrm{b}}$ quarks in the proton are the same. The total cross section splits equally between $\mathrm{tW^-}$ and $\mathrm{\bar{t}W^+}$ modes. Due to the tiny cross section at the Tevatron, it is almost certain that the first observation of tW channel will be at the LHC.

The $\mathrm{t\bar{t}}$ production process is the major background of this search. A small S/B ratio would inevitably enlarge the systematic uncertainties related to luminosity and $\mathrm{t\bar{t}}$ production cross section. A major component of this analysis consists of developing a ratio method to reduce these systematic uncertainties.

In this note we describe the analysis work done aiming to observe the tW process with the CMS detector. It is organized as follows: the signal and expected backgrounds are listed in section two, the Monte Carlo (MC) samples used for the study are described in section three, the trigger efficiencies are shown in section four, the event

[1)] Charge conjugation is implied in this note.

selection for the di-leptonic and semi-leptonic channels are explained in sections five and six, the expected signal and background yields as well as the ratio method to estimate the cross section are discussed in section seven, the methods and results of estimating systematic uncertainties are presented in section eight, the estimated significance is shown in section nine. Conclusions and future prospects are discussed in section ten.

2 Signal and Background

The $\mathrm{pp} \rightarrow \mathrm{tW}$ process results in a final state of two on-shell W bosons and a b quark. Similarly to the $\mathrm{t\bar{t}}$ analyses, we divide the final states into three categories based on the decay channel of the W bosons: di-leptonic, semi-leptonic, and fully hadronic. In this note we describe the analyses done on the first two categories. For the di-leptonic channel we only look for events with a high $\mathrm{p_T}$ electron and a high $\mathrm{p_T}$ muon of opposite charges. For the semi-leptonic channel we look for one high $\mathrm{p_T}$ charged lepton in the event, either an electron or a muon.

The nominal final state is ($\ell^+\ell^-\mathrm{E_T^{miss}b}$) and ($\ell^\pm\mathrm{E_T^{miss}bjj}$) for the di-leptonic and semi-leptonic modes, respectively. The dominant background for both channels is $\mathrm{t\bar{t}}$ production where a jet misses the acceptance or kinematic region. The jet multiplicity was considered the most effective discriminator between tW and $\mathrm{t\bar{t}}$ [9]. However, signal events often have extra jets due to calorimeter noise, underlying events and/or pile-ups. These extra jets make jet counting much less efficient in discriminating tW against $\mathrm{t\bar{t}}$. See figure 2 for the distribution of jet multiplicity in the tW and $\mathrm{t\bar{t}}$ events. It is clear that the number of jets does not peak at the expected place due to extra jets. A major part of the analysis work has been dedicated to the study of these extra jets.

Other backgrounds are t channel single top production, $\mathrm{Wb\bar{b}}$, W+jets, WW+jets, and to a lesser extent s channel single top production and multi-jet backgrounds. The leading order Feynman diagrams for selected background processes are shown in figure 3.

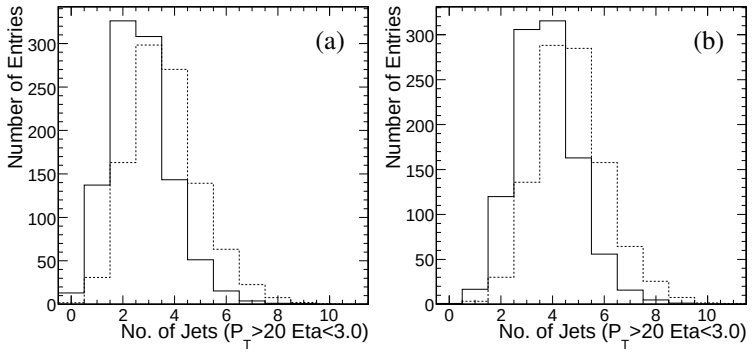

Figure 2: Distribution of number of jets with $\mathrm{p_T} > 20$ and $|\eta| < 3$ in Monte Carlo. (a): di-leptonic channel, (b): semi-leptonic channel. Solid histogram: tW signal, dashed histogram: $\mathrm{t\bar{t}}$.

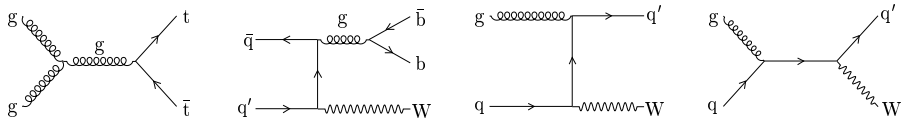

Figure 3: An incomplete list of leading order Feynman diagrams of background processes. From left to right: $\mathrm{t\bar{t}}$ production, $\mathrm{Wb\bar{b}}$, t channel W+jets, s channel W+jets.

3 Monte Carlo Samples

Various generators (TopReX [10], Pythia [11] and AlpGen [12]) are used to produce the samples for this study. TopReX is an NLO 2→N generator and is used to generate events with a single top quark or a pair of top quarks in the hard process. For detector simulation, most samples are simulated with the fast detector simulation program FAMOS [13] version 1_4_0 while some samples are simulated with detailed detector simulation program ORCA [14].

For the $\mathrm{t\bar{t}}$ background samples, TopReX + FAMOS are used in semi-leptonic mode, while Pythia + ORCA and

Pythia + FAMOS are used in the di-leptonic mode.

The generation of non-top background samples varies widely. The $\mathrm{Wb\bar{b}}$ sample is produced with TopReX + FAMOS, and we run FAMOS on an AlpGen W+jets ntuple to produce the W+jets sample. The WW+jets sample is produced with Pythia+FAMOS.

The softwares used to produce the samples and the size of each sample are listed in table 1.

Table 1: Samples used for the tW analysis. The generator and simulator are labelled as the following: T = TopReX 4_1_1, P = Pythia 6.325, A = AlpGen v205, F = FAMOS 1_3_2, F′ = FAMOS 1_4_0, O = ORCA 8_7_3.

Mode	**Semi-leptonic Analysis**	**Di-leptonic Analysis**
di-leptonic tW	180k TF′	80k TO, 120k TF
semi-leptonic tW	180k×2 TF′	
fully hadronic tW	180k TF′	-
di-leptonic $\mathrm{t\bar{t}}$	180k×2 TF′	900k PO, 250k PF
non di-leptonic $\mathrm{t\bar{t}}$	-	1.54M PO
semi-leptonic $\mathrm{t\bar{t}}$	180k+560k TF′	-
fully hadronic $\mathrm{t\bar{t}}$	180k TF′	-
leptonic t channel single top	100k TF′	40k TF
hadronic t channel single top	100k TF′	
leptonic s channel single top	100k TF′	
hadronic s channel single top	100k TF′	
leptonic Wbb	100k TF′	
hadronic $\mathrm{Wb\bar{b}}$	100k TF′	
W + 2 jets	576k AF′	
W + 3 jets	321k AF′	
W + 4 jets	87k AF′	
WW+jets di-leptonic	—	100k PF
WW+jets inclusive	—	100k PF
Multi-jet	1.4M PF′	2M PO

4 Triggers

Events are required to fire either the inclusive electron trigger or the inclusive muon trigger in the high level trigger (HLT) [15] whose efficiencies are studied in this work. Most of the samples used in the analysis are simulated with fast simulation program, and we use the samples with detailed simulation to compare the trigger efficiencies. For the di-leptonic channel, 7000 signal and 7000 $\mathrm{t\bar{t}}$ events with di-leptonic W decays are used. For the semi-leptonic channel, 66000 TopReX + ORCA signal events with semi-leptonic W decays are used to compare with the TopReX+FAMOS samples listed in table 1. The lepton flavours in the ORCA sample are not specified. As expected, the amount of e, μ and τ in the final states are found to be the same within statistical fluctualtion (21954 electrons, 22094 muons and 21952 tau leptons).

The trigger efficiencies obtained with the fast simulation and detailed simulation are found to agree reasonably well. The combined trigger efficiencies are 71.2% (di-leptonic channel), 47.7% (semi-leptonic channel) and 5.38% (fully hadronic). The total efficiency for tW is 18.9%.

5 Event Selection of the Di-Leptonic Channel

The signature of the di-leptonic tW events is two high $\mathrm{p_T}$ leptons (one electron and one muon for this analysis), large missing transverse energy, plus one b jet. In this section we describe the selection cuts of the di-leptonic channel.

5.1 Lepton quality requirements

The lepton quality cuts are listed in table 2. The electron related observables used are: E = energy deposition in the calorimeters, $\mathrm{E_{had}}$ = energy deposition in the hadron calorimeter, P = momentum of the associated track,

$\Delta\eta$(track.cluster) = the difference in pseudo-rapidity between the associated track and the calorimeter cluster, ΔR(track, cal) = the distance in the (η, ϕ) space between the associated track and the calorimeter cluster, $\mathrm{p_T}$ = the transverse momentum of the associated track, $\mathrm{E_T}$ = the transverse energy of the calorimeter, Δz = the difference in z (beam direction) between the associated track and the primary vertex of the event, Δr = the distance of closest approach of the associated track to the beam line in the transverse plane.

Table 2: Lepton quality cuts

Cut	**Comments**
Electrons	
E/P ≥ 0.8 $\mathrm{E_{had}}$/E ≤ 0.05 $\lvert\Delta\eta(\mathrm{track, cluster})\rvert \leq 0.005$ $\lvert$1/E - 1/P$\rvert \leq 0.8$ GeV^{-1} $\Delta R(\mathrm{track, cal}) \leq 0.15$	Standard electron identification cuts
$\lvert\Delta R$(all other $e^{\pm}$)$\rvert \geq 0.01$	photon conversion removal
$\sum \mathrm{p_T}$(near tracks†)/$\mathrm{E_T} \leq 0.05$	
Muons	
$\sum \mathrm{p_T}$(near tracks†)/$\mathrm{E_T} \leq 0.05$	

† see text for definition of near tracks.

The "near tracks" used in the lepton quality cut are defined as tracks that satisfy the following criteria: $0.015 < \Delta R < 0.35$, four or more tracker hits, $\Delta z < 0.4$ cm, $\Delta r < 0.1$ cm.

5.2 Jet quality requirements and extra jet reduction

The most significant difference between tW events and $\mathrm{t\bar{t}}$ events is the number of jets in the final state. It is one vs. two for the di-leptonic channel and three vs. four for the semi-leptonic channel. However, most of the time there are extra jets due to underlying events, pile-ups or calorimeter noise. This makes jet counting a much less efficient discriminator against the dominant $\mathrm{t\bar{t}}$ background. The same problem was also present in the $\mathrm{H \rightarrow WW \rightarrow \ell\nu\ell\nu}$ analyses [16].

The jets are reconstructed by an iterative cone algorithm [17] with a cone size ΔR = 0.5. In order to restore the effectiveness of jet counting the "extra jets" must be identified and excluded from the events. The extra jets are defined as the jets that do not match with any of the partons and leptons in the hard scattering. Several discriminating observables are found, however, a simple cut on the number of tracks with $\mathrm{p_T} > 1$ GeV inside the jet cone is found sufficient. A cut of $\mathrm{N_{track}} \geq 3$ has an 86.2% efficiency for true jets and rejects 71.8% of the extra jets.

5.3 Kinematic requirements

Charged leptons The charged leptons are required to be of opposite charge with different flavours (one electron and one muon) in order to suppress the $\mathrm{Z \rightarrow \ell^+\ell^-}$ and Drell-Yan backgrounds. A $\mathrm{p_T}$ cut at 20 GeV on both charged leptons reduces the backgrounds where one of the leptons comes from b decays: leptons not from W decays have a $\mathrm{p_T}$ distribution that peaks below 10 GeV, as shown in figure 4; instead, $\mathrm{p_T}$ distributions for the theree samples tW, $\mathrm{t\bar{t}}$ and WW are almost exactly the same.

This cut also avoids the region in which the $\mathrm{p_T}$ spectra produced by FAMOS and ORCA differ considerably.

Jets The events can be well classified by the number of b jets found and the $\mathrm{p_T}$ of the second jet (see figure 5). WW background is very important for single jet events with no b tagging, but is otherwise almost completely negligible; $\mathrm{t\bar{t}}$ background is present everywhere, and is dominating over any other sample for high jet 2 $\mathrm{p_T}$ in all the two b events. Events are selected as signal if they have exactly one jet, b tagged.

Isolation All the reconstructed objects are required to be isolated ($\Delta R > 0.5$) in order to suppress background caused by non primary leptons or hadrons misidentified as leptons.

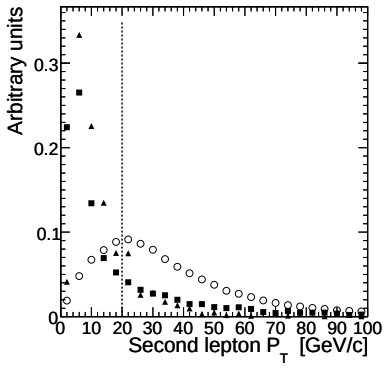

Figure 4: The $\mathrm{p_T}$ distribution of the second lepton. Empty circles: di-leptonic $\mathrm{t\bar{t}}$, squares: non di-leptonic $\mathrm{t\bar{t}}$, triangles: leptonic t channel single top.

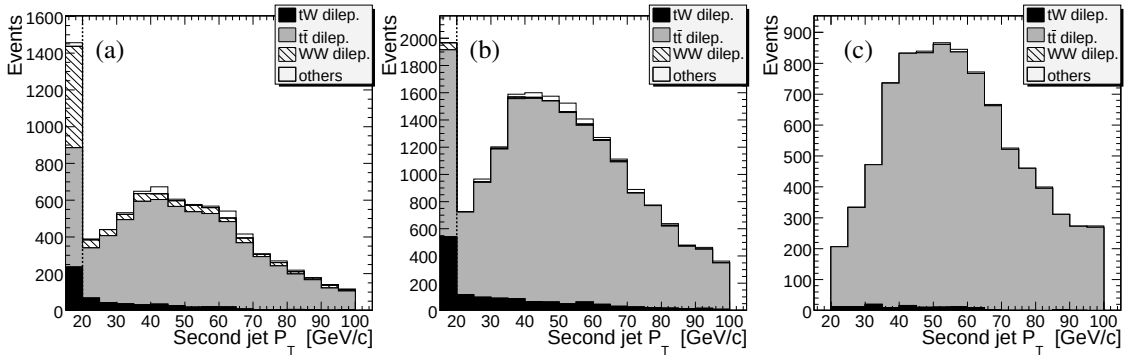

Figure 5: $\mathrm{p_T}$ of the second jet for events with 0, 1 and 2 b tagged jets; the vertical axis is numbers of events expected for 10 fb^{-1}; Leptonic t channel single top, non di-leptonic $\mathrm{t\bar{t}}$ and WW are grouped together under "other". The first column in the zero and one b plots are single jet events.

The kinematic cuts are summarized in table 3. The b-disc in the table is the b tagging discriminator [18].

Table 3: Kinematic cuts used in the di-leptonic channel.

Leptons
$\lvert\eta(e)\rvert < 2.4$, $\lvert\eta(\mu)\rvert < 2.1$
$\mathrm{p_{T1}} > 20$ GeV, $\mathrm{p_{T2}} > 20$ GeV
no other lepton with $\mathrm{p_T} > 5$ GeV
Jets
leading jet: $\lvert\eta\rvert < 2.4, \mathrm{p_T} > 60$ GeV, b-disc > 0
At most one extra jet
No other jets with $\mathrm{p_T} > 20$ GeV
Missing $\mathrm{E_T}$: $\mathrm{E_T^{miss}} > 20$ GeV

6 Event Selection of the Semi-Leptonic Channel

The signature of the semi-leptonic tW events is one high $\mathrm{p_T}$ electron or one muon, large missing transverse energy, one b jet, plus two more light quark jets from W decay. The hadronically decayed W boson can be the decay product of the top quark ("hadronic top events") or directly produced ("leptonic top events"). In this section we describe the selection cuts of the semi-leptonic channel.

6.1 Lepton quality requirements

The electron quality requirements of the semi-leptonic channel are the same as for the di-leptonic channel. No quality requirements are imposed on the muon candidates.

6.2 Jet quality requirements and extra jet reduction

The problem of the extra jets presented in 5.2 has been studied in detail for the semi-leptonic channel where more jets are expected in the events. The Monte Carlo samples used for the study are the TopReX + FAMOS tW signal sample and a single muon sample where one muon is fired by the particle gun generator into the detector in the simulation. The single muon sample is useful in finding jet quality variables that have discriminating power against extra jets.

We define extra jets as jets that don't match to the final state particles (i.e. partons and charged leptons) in the generator level. For the tW sample, the final state particles are b quarks, light quarks from W decays and charged leptons from W decays. For the single muon sample, all reconstructed jets are assumed to be calorimeter noise. Figure 6a shows the η distribution of true jets and extra jets in the TopReX + FAMOS tW signal sample. It exhibits two features: (1) there are a lot of extra jets, (2) the extra jets peak at small η. The "central" behavior can be understood by the threshold of forming a jet. The noises are expected to be uniform in η and have a tower energy spectrum more or less independent of η. However, since the seed threshold is on $\mathrm{E_T}$, it is more difficult for jets in the large η region to pass the threshold. This results in a suppression of extra jets in the large η region.

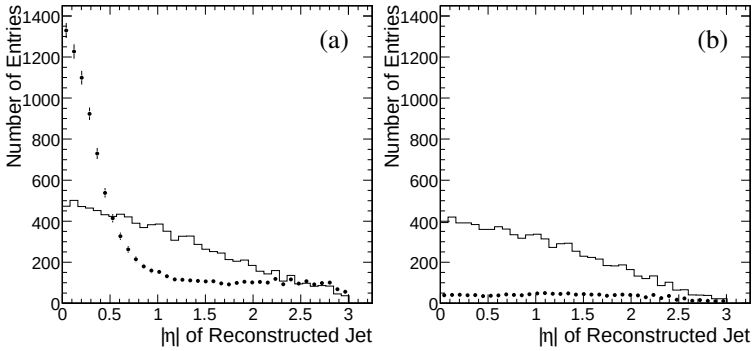

Figure 6: Distribution of the jet $|\eta|$ for true jets (histogram) and extra jets (circles) in the signal Monte Carlo sample before extra jet reduction (a), and after extra jet reduction (b). See text for details.

We consider five jet quality variables for extra jet reduction:

1. $\langle \Delta R \rangle$: tower energy weighted distance between tower and the jet axis,
2. $\mathrm{E_T^{max}}$: the maximum tower $\mathrm{E_T}$ in a cone of radius 0.5 (GeV),
3. $\mathrm{E_{0.3}/E_{0.5}}$: the ratio of tower energy between cones of 0.3 and 0.5,
4. N_{tower}: number of towers with $\mathrm{E_T}$ above 1 GeV in a 0.5 cone,
5. N_{track}: number of associated tracks from the b tagging algorithm [19].

To combine the discriminating powers of all the jet quality variables, a Fisher discriminant [20] in the five-dimensional space spanned by all the jet quality variables is formed to identify extra jets and true jets. The distributions of the jet quality variables and the Fisher discriminant are shown in figure 7.

Based on the value of the Fisher discriminant, each jet is classified as good, loose or bad. Table 4 shows the category cuts and efficiencies.

We compare the performance of the Fisher discriminant with the α parameter [21], which is defined as $\alpha \equiv \sum_i \mathrm{p_{T}}_i/\mathrm{E_T(jet)}$ where the summation runs over all tracks within a cone of radius ΔR = 0.5 to the jet axis with $\mathrm{p_T} > 0.9$ GeV and a track vertex consistent with primary event vertex. The performance of an $\alpha > 0.2$ cut is 70% efficient for true jets and 81% rejection on extra jets in the tW sample. a cut of -0.5 applied on the Fisher

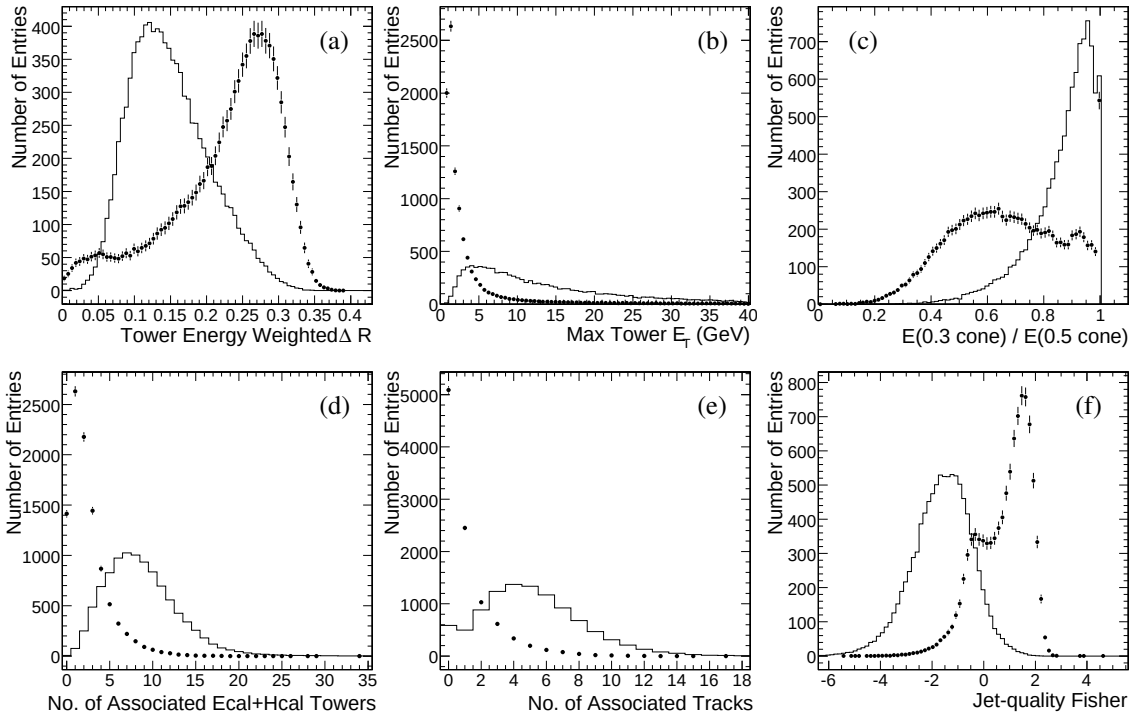

Figure 7: Distribution of jet quality variables $\langle \Delta R \rangle$ (a), $\mathrm{E_T^{max}}$ (b), $\mathrm{E_{0.3}/E_{0.5}}$ (c), N_{tower} (d), N_{track} (e) and the combined Fisher discriminant (f) in the tW signal Monte Carlo sample. The circles with error bars are extra jets and solid histogram are true jets.

Table 4: Categorization of jets based on the output of jet quality Fisher discriminant.

Category	**Fisher value**	**Real Jets (%)**	**Extra Jets (%)**
good jet	$F < -0.5$	84.3%	13.1%
loose jet	$-0.5 \leq F < 0.5$	13.4%	22.7%
bad jet	$F \geq 0.5$	2.3%	64.2%

discriminant would give 84% efficiency on true jets and rejects 87% of extra jets. The Fisher discriminant gives a big improvement on extra jet reduction. The resulting η distribution is shown in figure 6b.

Using all three categories carefully can give better performance than a single cut. All "bad" jets are removed from the jet list of the event. "Good" jets and "loose" jets are used in preselection and event reconstruction. The jet multiplicity after the extra jet reduction is shown in figure 8. It is seen that the number of good jets peaks at two and three jet bins for signal events, and three and four jet bins for $\mathrm{t\bar{t}}$ backgrounds.

6.3 Requirements on b tagging

Since the dominant background $\mathrm{t\bar{t}}$ has true b jets, the b tagging criteria only help in rejecting W+jets and multi-jet backgrounds. Nevertheless, we require that a jet must have b tagging discriminator greater than 2 to be considered a b-jet, in order to be consistent with the cut used in the estimation of b tagging systematic uncertainty [18]. The distribution of b tagging discriminator for the b-jet and 2 light quark jets from W decays are shown in figure 9.

For the light quark jets we require the b tagging discriminator to be less than zero.

6.4 Isolation cuts

The leptons and jets that pass quality cuts are ordered by $\mathrm{p_T}$. We then require that the leading lepton and three leading jets must be isolated from each other in (η, ϕ) space by $\Delta R > 0.5$.

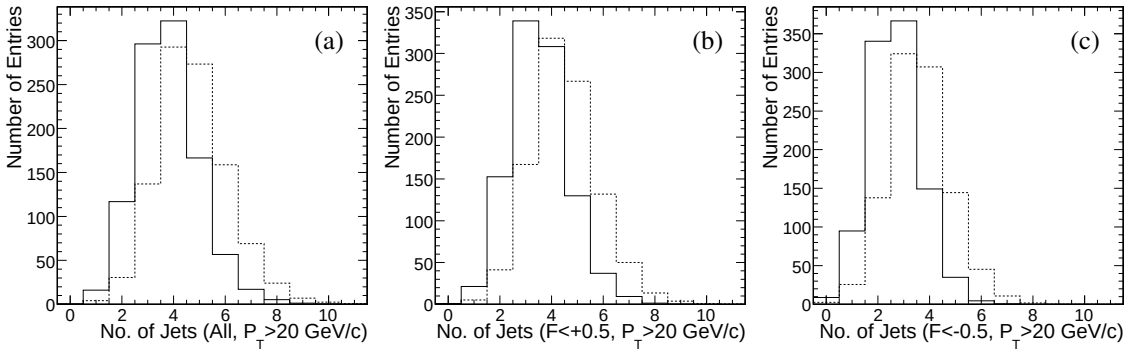

Figure 8: Jet multiplicity for all jets (a), good and loose jets (b), and good jets only (c). Solid histogram: semi-leptonic tW signal sample, dashed histogram: $\mathrm{t\bar{t}}$ backgrounds.

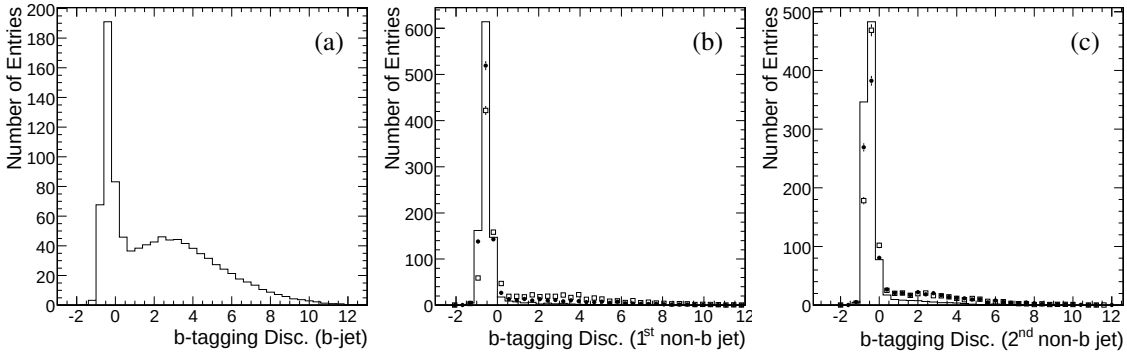

Figure 9: Distribution of the b tagging discriminator in the Monte Carlo samples for b jets (a), the leading light quark jets (b), and next-to-leading light quark jets (c). Histogram: tW semi-leptonic, circles: $\mathrm{t\bar{t}}$ semi-leptonic, and squares: $\mathrm{t\bar{t}}$ di-leptonic.

6.5 Kinematic requirements

The kinematic cuts are listed in table 5. We require one central electron or one central muon, large missing transverse energy, one b-tagged jet and two untagged jets. The presence of a good fourth jet would veto the whole event. The distributions of missing transverse energy of various processes are shown in figure 10.

Table 5: Kinematic selection cuts

Leptons
$\lvert\eta(e)\rvert < 2.4$, $\lvert\eta(\mu)\rvert < 2.1$
$\mathrm{p_T}(e) > 30$ GeV, $\mathrm{p_T}(\mu) > 20$ GeV
no other lepton $\mathrm{p_T} > 10$ GeV
Jets
extra jet removal: remove all bad quality jets
b-like jet: good quality, b-disc>2, $\lvert\eta\rvert < 3$, $\mathrm{p_T} > 35$ GeV
non-b-like jet: good quality, b-disc<0, $\lvert\eta\rvert < 3$, $\mathrm{p_T} > 35$ GeV
Jet counting: one b-like jet and two non-b-like jets
Jet veto: no other "good" or "loose" jets with $\mathrm{p_T} > 20$ GeV and $\lvert\eta\rvert < 3$
Missing $\mathrm{E_T}$: $\mathrm{E_T^{miss}} > 40$ GeV

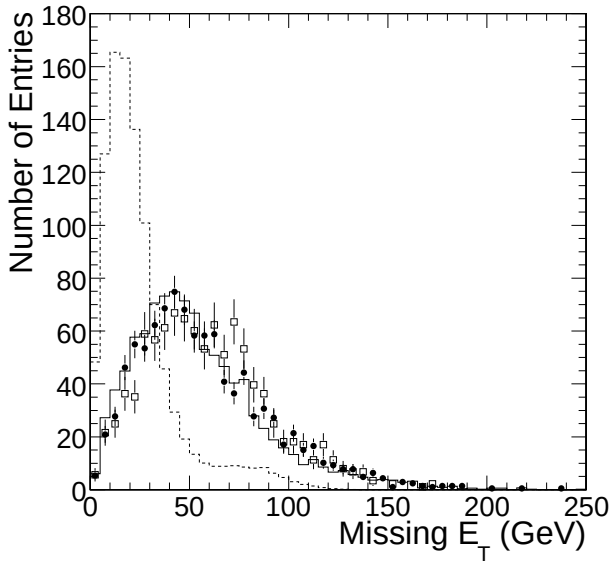

Figure 10: Distribution of $\mathrm{E_T^{miss}}$ in the Monte Carlo samples. Solid histogram: tW semi-leptonic, dashed histogram: multi-jet, circles: $\mathrm{t\bar{t}}$ semi-leptonic, squares: $\mathrm{t\bar{t}}$ di-leptonic.

6.6 Event reconstruction

6.6.1 Reconstruction of the hadronic W

In the semi-leptonic mode one W boson decays hadronically and can be fully reconstructed while the other W boson can not be fully reconstructed due to the undetected neutrino and unknown z-boost. The reconstructed invariant mass of two non-b-like jets $\mathrm{m_{jj}}$ and the transverse mass of the lepton and $\mathrm{E_T^{miss}}$ are shown in figure 11. We require the invariant mass of two non-b-like jets to pass a $\mathrm{m_{jj}} < 115$ GeV cut. For events that have a fourth jet (which must have failed the jet veto cut on jet quality, $\mathrm{p_T}$ or η), we require the invariant mass of the fourth jet with any of the non-b-like jets must be outside a window of ± 20 GeV relative to the W mass. This cut provides additional discriminating power against $\mathrm{t\bar{t}}$ with untagged b jets.

For W bosons that decay leptonically, we require that the transverse mass of the combined system of the charged lepton and the missing $\mathrm{E_T}$ must not exceed 120 GeV.

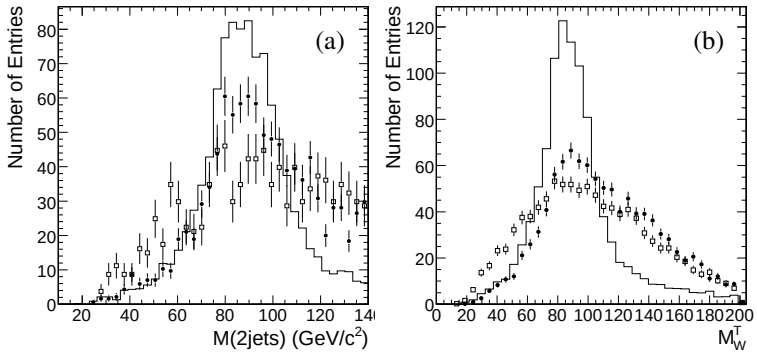

Figure 11: The invariant mass of two non-b-like jets (a) and transverse mass of lepton plus $\mathrm{E_T^{miss}}$ (b) in the Monte Carlo samples. Histogram: tW semi-leptonic, circles: $\mathrm{t\bar{t}}$ semi-leptonic, and squares: $\mathrm{t\bar{t}}$ di-leptonic.

6.6.2 Reconstruction of the leptonic W

We can reconstruct the leptonic W by finding the the z-component of the momentum of the neutrino $\mathrm{p_z}(\nu)$. It can be determined by assuming that $\vec{\mathrm{E}}_{\mathrm{T}}^{\mathrm{miss}} = \vec{\mathrm{p}}_{\mathrm{T}}(\nu)$ and requiring that the lepton and neutrino form a W. There are two solutions to the equation $(\mathrm{E}_\ell + \mathrm{E}_\nu)^2 - |\vec{\mathrm{p}}_\ell + \vec{\mathrm{p}}_\nu|^2 = \mathrm{m}_{\mathrm{W}}^2$. The equation does not always have real solutions due to the resolution and scale of $\mathrm{E_T^{miss}}$ in reconstructed events. We found that 37% of the reconstructed events have imaginary parts in the solutions. In such cases the real part is taken as the answer. For the remaining 63% of reconstructed events, the solution with smaller $|p_z|$ is taken as the answer, which is found to be correct in 67% of the cases in the generator level.

6.6.3 Reconstruction of the top quark: b-W pairing

With both the leptonic W and the hadronic W reconstructed, we can reconstruct the top quark by finding which of the two W is the product of top quark decay and pair it with the b-jet.

The variables used to find the right pairing are the $\mathrm{p_T}$ of (b, W) systems, the separation of the b-jet with each of the W in (η, ϕ) space, and the charges. The charge of a jet is defined as

$$q = \frac{\sum_i w_i \cdot q_i}{\sum_i w_i}$$

where the summation runs through all tracks in a cone of $\Delta R < 0.5$ with respect to the jet. q_i is the charge of the i-th track ($+1$ or -1), and the weight of that track is defined as

$$w_i \equiv \vec{\mathrm{p}}_i \cdot \vec{\mathrm{p}}_{\mathrm{jet}}.$$

The correlation between jet charge and the light quark that initiated the jet is not strong, but nonetheless we include it in the pairing determination.

With the jet charge defined, the charge of the hadronic W is taken to be the sum of jet charges of its decay products. The charge of the leptonic W is inherited from the charge of the lepton. The product of $q(\mathrm{W}) \cdot q(\mathrm{b})$ for each W is then used in the pairing analysis.

In all, six variables are used for pairing determination: $q(\mathrm{W}_h) \cdot q(\mathrm{b})$, $\mathrm{p_T}(\mathrm{W}_h + \mathrm{b})$, $\Delta R(\mathrm{W}_h, \mathrm{b})$, $q(\mathrm{W}_\ell) \cdot q(\mathrm{b})$, $\mathrm{p_T}(\mathrm{W}_\ell + \mathrm{b})$, and $\Delta R(\mathrm{W}_\ell, \mathrm{b})$. The distribution of these variables for leptonic top events and hadronic top eventsare shown in figure 12.

A Fisher discriminant in the six-dimensional space is used for discriminating leptonic top events from hadronic top events. The distribution of the pairing Fisher discriminant is shown in figure 13. A cut of of 0.56 is optimal in separating these two types of events, and 72% of the events are correctly paired. The reconstructed mass of the top quarks are shown in figure 13.

6.6.4 The signal region

We apply the following "global" cuts to further enhance the signal to background ratio:

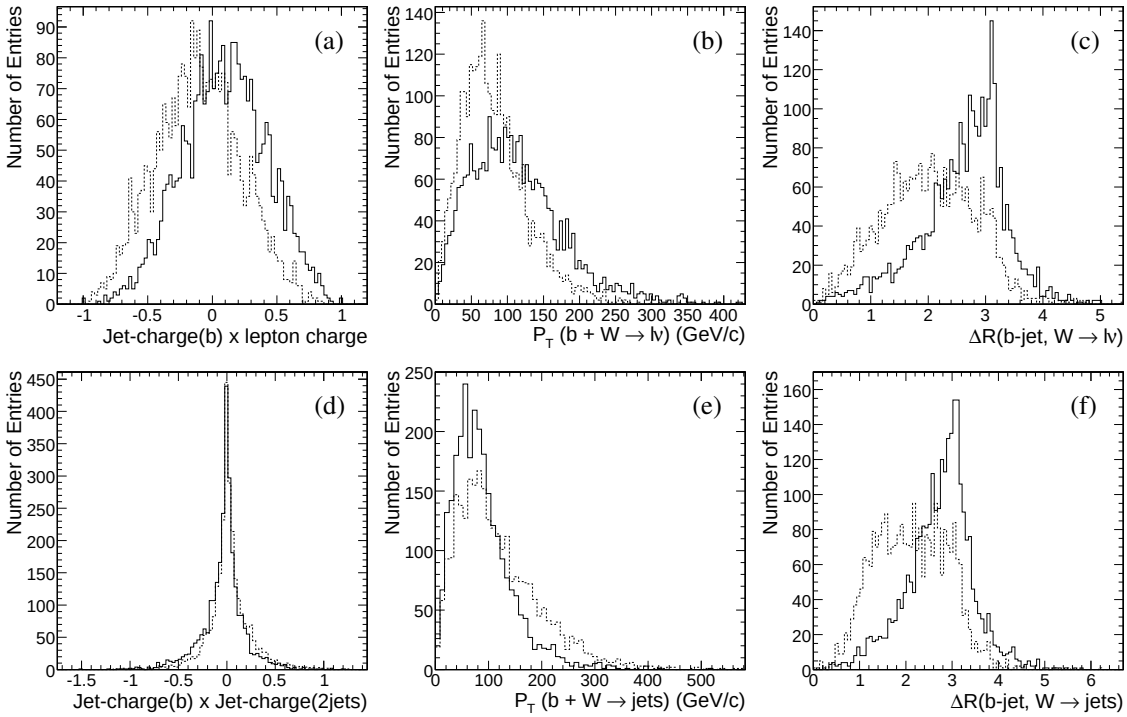

Figure 12: The distribution of variables used in b-W pairing analysis in the signal Monte Carlo: (a): $q(\mathrm{W}_\ell) \cdot q(\mathrm{b})$, (b): $\mathrm{p_T}(\mathrm{W}_\ell + \mathrm{b})$, (c): $\Delta R(\mathrm{W}_\ell, \mathrm{b})$, (d): $q(\mathrm{W}_h) \cdot q(\mathrm{b})$, (e): $\mathrm{p_T}(\mathrm{W}_h + \mathrm{b})$, and (f): $\Delta R(\mathrm{W}_h, \mathrm{b})$. Solid histogram: top to hadronic W events, dashed histogram: top to leptonic W events.

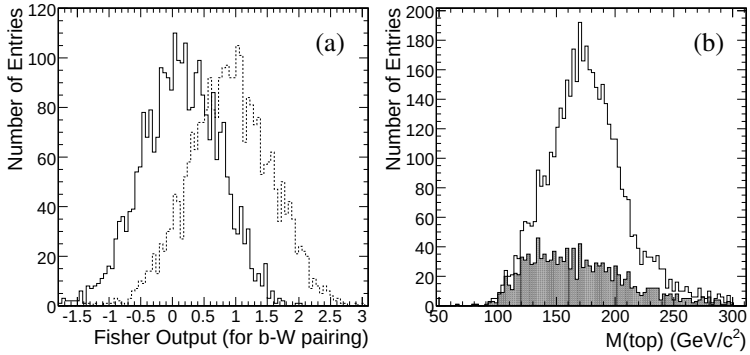

Figure 13: (a): the b-W pairing Fisher discriminant in the signal Monte Carlo. Solid histogram: leptonic top events, dashed histogram: hadronic top events. (b): The distribution of reconstructed top quark mass. The input top quark mass to the sample is 175 GeV. Empty histogram: all pairings, filled histogram: incorrect pairings.

- $\mathrm{p_T}$ of the reconstructed tW system: $\mathrm{p_T}(\mathrm{t} + \mathrm{W}) < 60$ GeV.
- Scalar sum of transverse energies $\mathrm{H_T}$: $\mathrm{H_T} < 850$ GeV.
- Reconstructed top quark mass: $110 < \mathrm{m(t)} < 230$ GeV.
- $\mathrm{p_T}$ of the reconstructed top quark: $20 < \mathrm{p_T(t)} < 200$ GeV.

The distributions of these variables are shown in figure 14.

7 Cross Section Measurement

The Standard Model predicts that the cross section of $\mathrm{pp} \to \mathrm{tW}$ is about 60 pb, which is only 7% of the cross section of the $\mathrm{pp} \to \mathrm{t\bar{t}}$ background. In this section we show the summary table of efficiencies and expected yields

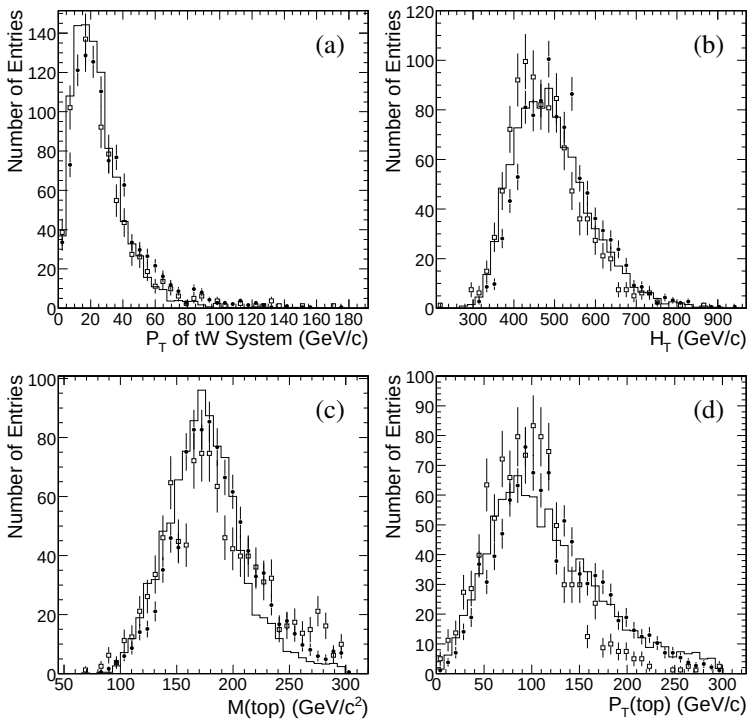

Figure 14: The global variables used for defining the semi-leptonic signal region. (a): $\mathrm{p_T(tW)}$, (b): $\mathrm{H_T}$, (c): $\mathrm{m(t)}$, (d): $\mathrm{p_T(t)}$. The histograms are tW signal, the solid circles are semi-leptonic $\mathrm{t\bar{t}}$ and the empty squares are di-leptonic $\mathrm{t\bar{t}}$.

for 10 fb^{-1} of data for both channels after a description of the special treatment used to obtain multi-jet background yields. A simple analysis of uncertainties on cross section follows, and it shows that a large B/S factor amplifies the uncertainties. A ratio method employed to address this problem is then described.

7.1 The methods for estimating efficiencies

The efficiency of the selection cuts on a process is determined in Monte Carlo samples by finding the number of events that survive all the cuts, and the efficiency is simply the ratio between selected events and the sample size $\epsilon = \mathrm{N_{pass}/N_{sample}}$. For background processes whose Monte Carlo sample is not large enough to have at least one event passing the whole selection criteria, one of the two following methods is used to estimate the expected yields.

Upper limit method This is used for processes with cross sections below 1 nb or so. One event is assumed to pass all the cuts and the corresponding yield is obtained as an upper limit, which usually is small.

Combined efficiency method This is used for multi-jet background. It has a huge cross section and tiny efficiency, therefore a big sample would be needed to determine the efficiency. The statistics of available Monte Carlo DSTs is not sufficient, and zero events pass the whole event selection cuts in both the di-leptonic channel and semi-leptonic channel.

The procedure of the combined efficiency method is the following:

1. A set of (almost) independent and inclusive cut groups are defined;
2. Efficiencies for signal and background for each cut group are determined individually with the available MC sample;
3. A "combined efficiency" is calculated as the product of the efficiencies determined in the previous step, neglecting the correlations among them;

The cut groups for the di-leptonic and semi-leptonic channel are listed in table 6. The results on the efficiencies and expected yields are shown in table 7 and 8.

Table 6: Cut groups used to determine the yield of multi-jet background in the di-leptonic and semi-leptonic channels.

Di-leptonic channel	
one e	the electron selection cuts
one μ	the muon selection cuts
$\mathrm{E_T^{miss}}$	$\mathrm{E_T^{miss}} > 20$ GeV
jets	jet selection, veto and b tagging cuts
Semi-leptonic channel	
jets	jet selection and veto cuts
lepton	lepton selections
kine.	kinematic requirements
srbt	signal region and b tagging requirements

Table 7: Estimation of multi-jet yield for the di-leptonic channel.

		Combined Efficiencies				
$\hat{p}_T$ (GeV)	σ **(pb)**	1 e	+1 μ	+$\mathrm{E_T^{miss}}$	+jets	**Yield**
15–20	1.46×10^{9}	2.22×10^{-5}	4.94×10^{-10}	1.10×10^{-14}	2.44×10^{-19}	3.55×10^{-6}
20–30	6.32×10^{8}	1.11×10^{-5}	6.17×10^{-10}	9.60×10^{-14}	1.07×10^{-18}	6.74×10^{-6}
30–50	1.63×10^{8}	3.23×10^{-5}	1.39×10^{-9}	1.03×10^{-12}	4.43×10^{-17}	7.21×10^{-5}
50–80	2.16×10^{7}	1.32×10^{-4}	2.21×10^{-8}	2.37×10^{-10}	1.39×10^{-13}	3.01×10^{-2}
80–120	3.08×10^{6}	3.61×10^{-4}	1.90×10^{-7}	1.12×10^{-8}	3.48×10^{-11}	1.07×10^{0}
120–170	4.93×10^{5}	4.79×10^{-4}	3.50×10^{-7}	6.02×10^{-8}	4.46×10^{-10}	2.20×10^{0}
170–230	1.01×10^{5}	6.69×10^{-4}	9.82×10^{-7}	3.28×10^{-7}	4.28×10^{-9}	4.31×10^{0}
230–300	2.45×10^{4}	7.06×10^{-4}	1.42×10^{-6}	6.83×10^{-7}	1.27×10^{-8}	3.12×10^{0}
300–380	6.24×10^{3}	7.70×10^{-4}	2.20×10^{-6}	1.31×10^{-6}	3.22×10^{-8}	2.01×10^{0}
380–470	1.78×10^{3}	6.63×10^{-4}	2.74×10^{-6}	1.85×10^{-6}	5.05×10^{-8}	8.99×10^{-1}
470–600	6.83×10^{2}	7.07×10^{-4}	3.88×10^{-6}	2.86×10^{-6}	8.84×10^{-8}	6.04×10^{-1}
600–800	2.04×10^{2}	9.47×10^{-4}	7.50×10^{-6}	5.92×10^{-6}	1.98×10^{-7}	4.04×10^{-1}
800–1000	3.51×10^{1}	8.89×10^{-4}	9.44×10^{-6}	7.79×10^{-6}	2.67×10^{-7}	9.39×10^{-2}
Sum						14.7

For the di-leptonic channel, the multi-jet background is efficiently suppressed, as the estimated yield is only 14.7 events for 10 fb^{-1}. In addition the cuts were chosen as to select not just the signal events, but also the events which will end in the region used to normalize the $\mathrm{t\bar{t}}$ background, as we want to control the multi-jet contamination to that events too. To estimate the amount of events that pass the whole selection for signal we can calculate the combined efficiency also for the signal using the same procedure, and then normalize the final efficiency assuming that the ratio between final efficiency and combined efficiency is the same for multi-jet and for signal: the final yield is 5.6 events, 1% of the expected signal yield.

The $\mathrm{E_T^{miss}}$ cut rejects mostly low $\hat{\mathrm{p}}_\mathrm{T}$ jets; if this cut is not used the final background contamination is still small (below 3% of the signal). The isolation requirement for for electrons appears to be stronger than for muons due to additional cuts on $\mathrm{E_{had}/E}$ and $\mathrm{E/P}$. Applying tighter isolation cuts to the muons should then allow an even greater suppression of the multi-jet background.

For the semi-leptonic channel, it is found that the cuts are not totally uncorrelated. Multiplying the efficiencies except the last two results in an effective cross section of 36.2 pb, much larger than the 0.85 pb obtained by applying cuts in series. This is an indication that the cuts have anti-correlations, i.e., the efficiency of latter cuts is reduced a lot with the presence of prior cuts. That in turn means the final yield of 507.5 events is likely an over-estimate. We keep it in the table to be conservative.

Table 8: Estimation of multi-jet yield for the semi-leptonic channel.

		Combined Efficiencies					
$\hat{p}_T$ (GeV)	σ **(pb)**	presel.	+jets & vetos	+lepton	+kine.	+signal region & b tag	**Yield**
50–80	2.16×10^{7}	1.60×10^{-4}	3.85×10^{-7}	4.81×10^{-8}	2.44×10^{-9}	5.01×10^{-11}	1.08×10^{1}
80–120	3.08×10^{6}	3.40×10^{-4}	1.99×10^{-5}	6.44×10^{-6}	4.51×10^{-7}	1.17×10^{-8}	3.59×10^{2}
120–170	4.93×10^{5}	9.30×10^{-4}	6.91×10^{-5}	1.19×10^{-5}	6.78×10^{-7}	2.43×10^{-8}	1.20×10^{2}
170–230	1.01×10^{5}	1.76×10^{-3}	2.45×10^{-4}	4.42×10^{-5}	1.43×10^{-6}	1.67×10^{-8}	1.69×10^{1}
230–300	2.45×10^{4}	3.15×10^{-3}	4.96×10^{-4}	1.22×10^{-4}	2.82×10^{-6}	5.32×10^{-9}	1.30×10^{0}
300–380	6.24×10^{3}	4.53×10^{-3}	7.32×10^{-4}	2.00×10^{-4}	2.38×10^{-6}	5.45×10^{-10}	*negligible*
380–470	1.78×10^{3}	6.43×10^{-3}	1.02×10^{-3}	2.73×10^{-4}	4.13×10^{-7}	2.21×10^{-12}	*negligible*
470–600	6.83×10^{2}	8.92×10^{-3}	1.34×10^{-3}	4.57×10^{-4}	3.63×10^{-8}	1.33×10^{-13}	*negligible*
600–800	2.04×10^{2}	1.10×10^{-2}	1.77×10^{-3}	6.44×10^{-4}	8.37×10^{-9}	4.49×10^{-15}	*negligible*
800–1000	3.51×10^{1}	1.32×10^{-2}	1.91×10^{-3}	6.91×10^{-4}	6.16×10^{-9}	1.56×10^{-14}	*negligible*
Sum							507.5

7.2 Summary of efficiencies and expected yields

The efficiency results are converted to effective cross sections by multiplying the production cross sections of each process. The effective cross sections, as well as the expected yields with 10 fb^{-1} of data for all signal and background samples considered, are shown in table 9 and table 10 for di-leptonic and semi-leptonic channels, respectively. The signal to background ratio for 10 fb^{-1} of integrated luminosity is found to be 562/1532 = 0.37 for the di-leptonic channel and 1699/9256 = 0.18 for the semi-leptonic channel.

Table 9: Summary of effective cross sections at each stage of the analysis for the di-leptonic channel. All values are in picobarns except that the last row is the expected number of events for 10 fb^{-1}. The table cells with a † symbol indicates the yield is estimated with the upper limit method or the combined efficiency method. See text for details.

	tW **dil.**	$\mathrm{t\bar{t}}$ **dil.**	$\mathrm{t\bar{t}}$ **oth.**	**WW dil.**	**WW oth.**	**t ch. lept.**	**Multi-jet**
Production	6.667	92.222	742.885	11.111	88.889	81.667	$2.28 \cdot 10^{9}$
HLT	4.865	74.090	327.247	7.674	27.259	41.409	$1.45 \cdot 10^{6}$
$2\ \ell$	1.944	25.150	5.117	2.574	0.226	2.309	$2.07 \cdot 10^{3}$
Lepton $\mathrm{p_T}$, η	0.675	7.917	0.118	0.543	0.012	0.098	0.002
≤ 1 extra jet	0.459	6.573	0.105	0.416	0.010	0.067	0.002
Jet $\mathrm{p_T}$, η	0.298	5.210	0.096	0.327	0.004	0.033	0.000
≥ 1 b-jet	0.205	4.219	0.068	0.019	0.000	0.022	0.000
$\mathrm{E_T^{miss}} > 20$	0.190	3.973	0.064	0.019	0.000	0.020	0.000
≤ 2 jet	0.156	2.904	0.032	0.016	0.000	0.012	0.000
Final select.	0.056	0.143	$0.000^{\dagger}$	0.006	$0.000^{\dagger}$	$0.000^{\dagger}$	$0.000^{\dagger}$
Expected events	562	1433	$\leq 4.3^{\dagger}$	55	$\leq 10^{\dagger}$	$\leq 20^{\dagger}$	$\leq 10^{\dagger}$

7.3 Cross section and analysis on uncertainties

The cross section is calculated as

$$\sigma = \frac{S}{\epsilon\mathcal{L}} = \frac{N-B}{\epsilon\mathcal{L}}$$

where

S = number of observed signal events,

N = total number of observed events,

B = expected number of background events,

ϵ = estimated signal efficiency,

$\mathcal{L}$ = integrated luminosity.

Table 10: Summary of cross section times branching ratio times efficiencies at each stage of the analysis for the semi-leptonic channel. All values are in picobarns except that the last row is the expected number of events.

	tW	$\mathrm{t\bar{t}}$	**t ch.**	**s ch.**	**Wbb**	**W2j**	**W3j**	**W4j**	**Multi-jet**
Production cross section σ	60	833	245	10	300	7500	2166	522	9.73×10^9
High Level Trigger	18.9	263.9	39.5	1.52	34.0	1006	300	73	1.86×10^5
Preselection and isolation	9.05	179.4	12.0	0.54	2.15	52	35	12	1325
jet & lepton p_T cuts, jet veto	1.28	18.5	1.31	0.046	0.061	0.60	4.9	1.0	4.23
b-tagging	0.669	6.13	0.476	0.013	0.016	0.10	0.99	0.26	0.85
kinematical cuts	0.223	0.987	0.047	0.002	0.003	0.017	0.101	0.008	$0.105^\dagger$
Signal region cuts	0.170	0.762	0.035	0.001	0.001	0.013	0.054	0.008	$0.051^\dagger$
Expected yield for 10 fb^{-1}	1699	7624	351	14	10	130	539	80	508

† Estimated with the combined efficiency method. See section 7.1 for details.

A simple propagation of error shows that the relative uncertainty of cross section is

$$\frac{\Delta_\sigma}{\sigma} = \frac{\Delta_\epsilon}{\epsilon} \oplus \frac{\Delta_\mathcal{L}}{\mathcal{L}} \oplus (\frac{B}{S}+1)\frac{\Delta_N}{N} \oplus \frac{B}{S}\frac{\Delta_B}{B} \tag{1}$$

where the $\oplus$ means addition in quadrature. Since the S/B of this analysis is quite small, the last two terms are "amplified" by a large B/S.

The systematic uncertainties of the cross section strongly depend on how the number of background events is estimated. Traditionally the selection efficiency on the backgrounds and theoretical calculation of the background cross sections are used to find the expected number of background events in every background channel:

$$B = \sum_i B_i = \sum_i \epsilon_i \cdot \sigma_i \cdot \mathcal{L}.$$

The error can be written as

$$\Delta_B = \sum_i^\oplus \Delta_{B_i} = \sum_i^\oplus B_i(\frac{\Delta_{\epsilon_i}}{\epsilon_i} \oplus \frac{\Delta_{\sigma_i}}{\sigma_i} \oplus \frac{\Delta_\mathcal{L}}{\mathcal{L}}) = \sum_i^\oplus B_i(\frac{\Delta_{\epsilon_i}}{\epsilon_i} \oplus \frac{\Delta_{\sigma_i}}{\sigma_i}) \oplus \left(\sum_i^\oplus B_i\right)\frac{\Delta_\mathcal{L}}{\mathcal{L}}.$$

The symbol $\sum^\oplus$ means summation in quadrature. It follows from Eq. (1) that there is a multiplicative factor of $(\sum_i^\oplus B_i/S+1)$ for the luminosity uncertainty. Using the expected yields in table 10, we can estimate that a 5% luminosity uncertainty results in a 21% $\Delta\sigma/\sigma$, and a 9% uncertainty on $\mathrm{t\bar{t}}$ cross section results in 50% $\Delta\sigma/\sigma$. These uncertainties are too large to be acceptable. Therefore we use a *ratio method* described below in order to cancel systematic uncertainties from the dominant background $\mathrm{t\bar{t}}$.

7.4 The ratio method

In the ratio method, we single out the dominant background channel ($\mathrm{t\bar{t}}$) for a special treatment. We define a $\mathrm{t\bar{t}}$ control region that has a high purity of $\mathrm{t\bar{t}}$ events. The initial intention was to use the number of events in the $\mathrm{t\bar{t}}$ control region to normalize the $\mathrm{t\bar{t}}$ backgrounds in the signal region. However, due to the similarity in kinematics between the tW events and the $\mathrm{t\bar{t}}$ events, we found that it is difficult to have a $\mathrm{t\bar{t}}$ control region without non-negligible tW events. The ratio method then was extended to contain two ratios: the ratio of efficiencies in the two region for tW (R_{tW}), and the ratio for $\mathrm{t\bar{t}}$ ($R_{\mathrm{t\bar{t}}}$).

The formulation of the method is simple. The number of events in a region is the sum of expected events from tW, $\mathrm{t\bar{t}}$, and other backgrounds (t channel and s channel single top quark events, $\mathrm{Wb\bar{b}}$, W+jets and multi-jets):

$$\begin{aligned} N_s &= N_s^{\mathrm{tW}} + N_s^{\mathrm{t\bar{t}}} + N_s^o, \\ N_c &= N_c^{\mathrm{tW}} + N_c^{\mathrm{t\bar{t}}} + N_c^o. \end{aligned} \tag{2}$$

In equation (2) the N_s and N_c are assumed to be observed in real data. N_s^o and N_c^o, the number of "other" backgrounds, are estimated with luminosity, theoretical cross section and efficiencies determined in Monte Carlo samples. The remaining four terms are solved by using the efficiency ratios which satisfy the following equations:

$$\begin{aligned} R_{\mathrm{tW}} &\equiv \left.\frac{\epsilon_c^{\mathrm{tW}}}{\epsilon_s^{\mathrm{tW}}}\right|_{\mathrm{MC}} = \frac{N_c^{\mathrm{tW}}}{N_s^{\mathrm{tW}}} \\ R_{\mathrm{t\bar{t}}} &\equiv \left.\frac{\epsilon_c^{\mathrm{t\bar{t}}}}{\epsilon_s^{\mathrm{t\bar{t}}}}\right|_{\mathrm{MC}} = \frac{N_c^{\mathrm{t\bar{t}}}}{N_s^{\mathrm{t\bar{t}}}} \end{aligned}$$

The events in the signal region can then be readily solved as

$$\begin{cases} N_s^{\mathrm{tW}} &= \frac{R_{\mathrm{t\bar{t}}}(N_s - N_s^o) - (N_c - N_c^o)}{R_{\mathrm{t\bar{t}}} - R_{\mathrm{tW}}} \\ N_s^{\mathrm{t\bar{t}}} &= \frac{(N_c - N_c^o) - R_{\mathrm{tW}}(N_s - N_s^o)}{R_{\mathrm{t\bar{t}}} - R_{\mathrm{tW}}} \end{cases} \tag{3}$$

With the number of events of tW and $\mathrm{t\bar{t}}$ processes found with equation (3), the signal yield S, background yield B and cross section of the $\mathrm{pp} \to \mathrm{tW}$ process σ are then simply

$$\begin{cases} S &= N_s^{\mathrm{tW}}, \\ B &= N_s^{\mathrm{t\bar{t}}} + N_s^o, \\ \sigma &= \frac{S}{\epsilon_s^{\mathrm{tW}} \mathcal{L}}. \end{cases} \tag{4}$$

If the kinematics of the signal and control regions are similar, it is expected that systematic uncertainties from PDF, b tagging and jet energy scale can cancel at least partially with the ratio method, and the luminosity uncertainty only contributes to the "other" backgrounds and the signal, not the $\mathrm{t\bar{t}}$ background. The $\mathrm{t\bar{t}}$ cross section is not an input to this measurement so it is not a source of systematic uncertainties.

How well the ratio method performs is determined by the systematic uncertainties. To cancel systematic uncertainties better the kinematics in the control region and the signal region should be similar except that the control region has one more jet. Another important point is that the $\mathrm{t\bar{t}}$ purity must be high in the control region. The control region is defined as the following for di-leptonic and semi-leptonic channels, respectively.

Di-leptonic

- Lepton and jet quality cuts: the same as the signal region.
- Lepton selection: the same as the signal region.
- Jet kinematics: a second jet is required, $20 < \mathrm{p_T}$ (GeV) < 80, again central ($|\eta| < 2.4$) and b-tagged (b-discriminant > 0). No other jets with $\mathrm{p_T} > 20$ GeV are allowed.

The background region is found to be filled by 97.9% di-leptonic $\mathrm{t\bar{t}}$, 0.4% from other $\mathrm{t\bar{t}}$ decays, 1.6% di-leptonic tW, and 0.1% for leptonic t channel single top while the WW+jets yield is negligible.

Semi-leptonic

- Lepton and jet quality cuts: the same as the signal region.
- Lepton selection: the same as the signal region.
- Jet kinematics: the same η range as the signal region, but require two jets with $\mathrm{p_T} > 30$ GeV, two more jets with $\mathrm{p_T} > 20$ GeV, and no bad jets with $\mathrm{p_T} > 20$ GeV.
- b tagging: require one of the two high-$\mathrm{p_T}$ jets is b-tagged (b-discriminant > 2), and require both low-$\mathrm{p_T}$ jets to be not tagged (b-disc < 0).
- The $\mathrm{b} - \mathrm{W}$ pairing is done in the same way, with 72% correct pairing fraction.

It is found that the $\mathrm{t\bar{t}}$ purity in the background region is 93.9% from 27194 selected events. The non-$\mathrm{t\bar{t}}$ events are mainly composed of W+jets (2.8%), tW (2.0%) and t channel single top (1.2%). The ratio of efficiencies are found to be (R_{tW}, $R_{\mathrm{t\bar{t}}}$) = (0.224, 5.39) for di-leptonic channel and (0.319, 3.31) for semi-leptonic channel, respectively.

We verify the ratio method and its implementation by generating the number of tW events in signal and control regions according to an input cross section with a Poisson fluctuation and use the ratio method to get the cross section back. The result is shown in figure 15, which shows that the ratio method returns the input cross section.

The systematic uncertainties with the ratio method are described in the next section.

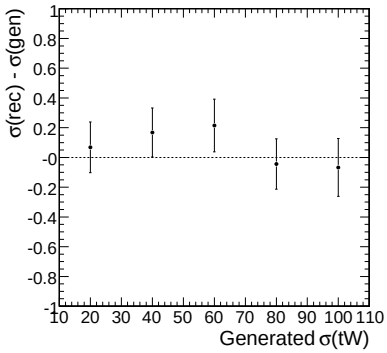

Figure 15: The measured cross section in toy Monte Carlos versus the input cross section.

8 Systematic Uncertainties

The estimate of the systematic uncertainty of cross section $\sigma(\mathrm{pp} \to \mathrm{tW})$ with the ratio method is not too different from the normal method. A block diagram of the ratio method and associated systematic uncertainty estimation is shown in figure 16, which describes the analysis in a pictorial way. First the cuts for signal and control regions

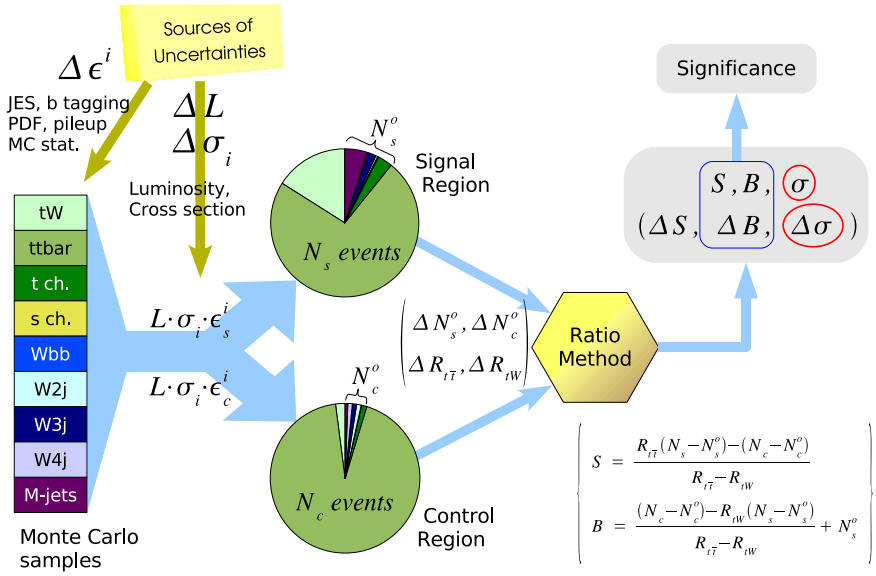

Figure 16: Block diagram of the ratio method and associated systematic uncertainties. See text for details.

are applied to every Monte Carlo sample to determine the efficiencies ϵ_s^i and ϵ_c^i where i is the index of Monte Carlo samples. The efficiency ratios $R_{\mathrm{tW}} = \epsilon_c^{\mathrm{tW}}/\epsilon_s^{\mathrm{tW}}$ and $R_{\mathrm{t\bar{t}}} = \epsilon_c^{\mathrm{t\bar{t}}}/\epsilon_s^{\mathrm{t\bar{t}}}$ are then determined. The composition of events in the signal and control regions are found by calculating the expected yields in each region: $N_s^i = \mathcal{L} \cdot \sigma_i \cdot \epsilon_s^i$ and $N_c^i = \mathcal{L} \cdot \sigma_i \cdot \epsilon_c^i$. The size of the signal region and control region are then simply a sum of yields: $N_s = \sum_i N_s^i, N_c = \sum_i N_c^i$. The yields are fed into the ratio method to find the nominal values of (S_0, B_0, σ_0), which are treated as the "*truth*" in the analysis.

For estimating the systematic uncertainties, the sources of uncertainties are used to vary (1) the events which leads to efficiency changes, or (2) the input background cross section, or (3) the integrated luminosity. The size of both regions N_s and N_c are kept fixed at all times during the analysis. Whenever an uncertainty source is varied, the resulting efficiencies, integrated luminosity or cross sections are considered as the "*best estimates*". The best estimates are used in the ratio method to get the output (S, B, σ). The difference $\Delta\sigma \equiv \sigma - \sigma_0$ is taken as a systematic uncertainty of cross section due to this variation of uncertainties source. Similarly the term $\Delta_B \equiv B - B_0$ is an estimate of the systematic uncertainty of background yields, which is used in the significance estimation, see section 9 for further details.

We consider the following sources of systematic uncertainties of the cross section measurement: Luminosity, theoretical calculation of background cross sections, jet energy scale, parton distribution functions, b tagging efficiency, Monte Carlo statistics, and amount of pile-up events. In the following subsections the details of determination of the contribution to the total systematic uncertainty from each source is described.

8.1 Luminosity

The systematic uncertainty due to luminosity uncertainty is estimated by varying the integrated luminosity for calculation of the yields N_s^o and N_c^o in equation (3) to find the change in the cross section. The luminosity uncertainty for 10 fb^{-1} is expected to be 5% [22]. Such an uncertainty produces 5.4% and 7.8% systematic uncertainty on the cross section for the di-leptonic and the semi-leptonic channels, respectively.

8.2 Theoretical uncertainties

The theoretical uncertainties considered arise from uncertainties on the cross sections of various background processes. Because the $\mathrm{t\bar{t}}$ cross section does not appear in the ratio method, the contribution comes from t channel single top, s channel single top, $\mathrm{Wb\bar{b}}$, W+jets and WW+jets. We shift the corresponding cross section values by 1σ in equation (3) and find the change in the cross section. The result is 0.8% for t channel single top and 3.1% for W+jets in the semi-leptonic channel, 1% for WW+jets in the di-leptonic one. It is found to be negligible for s channel single top and $\mathrm{Wb\bar{b}}$.

8.3 Jet energy scale

The uncertainty due to jet energy scale is estimated by shifting $\mathrm{E_T}$ of every jet to $\mathrm{E_T}' = (1+\lambda)\mathrm{E_T}$ to find the new efficiencies for the signal and control regions. We take $\lambda = \pm 2.5\%$ for $\mathrm{E_T} \geq 50$ GeV, $\lambda = \pm 5\%$ for $\mathrm{E_T} = 25$ GeV, and interpolate linearly between 25 and 50 GeV [23]. The result is 19.7% for di-leptonic channel and 9.4% for the semi-leptonic channel.

8.4 B tagging efficiency

The documented systematic uncertainty on b tagging efficiency is 4% in the barrel and 5% in the endcaps [18]. In the di-leptonic channel the uncertainty of b tagging efficiency is implemented in the events by randomly choosing 4% of untagged jets to be tagged and vice versa. The resulting change in cross section, $\pm 8.7\%$, is the systematic uncertainty.

In the semi-leptonic channel the b tagging uncertainty is modelled by changing the b-discriminant value up and down by a value δ which produces the required shift in b tagging efficiencies. We then find the change of event counts in the signal region and control region.

The value of δ is found to be $-0.1814/+0.1898$ for barrel and $-0.1920/+0.1877$ for endcap regions. The systematic uncertainty is found to be 3.6% for the semi-leptonic channel.

8.5 Parton Distribution Functions

The systematic uncertainties due to parton distribution functions are traditionally estimated by using a different PDF to generate the Monte Carlo samples and find the difference in cross section between samples. This requires a large amount of storage space and very long CPU time.

The PRS Generator Tools group has recommended a new way to estimate the PDF uncertainties which is based on the Hessian method with LHAPDF [24], In short, the CTEQ61 PDF has 20 parameters to describe all parton distribution functions of a proton, denoted as $\vec{a} = (a_1, a_2, ...a_{20})$. The correlations among parameters are zero because the covariant matrix is diagonalized. Each generated event has a probability proportional to the differential cross section in the vicinity of the phase space of the event. The differential cross section changes if the parameters change. Therefore we can estimate the change of cross section by re-weighting the generated events with weights defined as

$$w_i^{\pm} = \frac{\mathrm{PDF}(..., a_i^{\pm}, ...)}{\mathrm{PDF}(\vec{a})}$$

where a_i^+ is the value of a_i varied by one sigma upwards and a_i^- similarly for downward variation.

We examined the weights in the semi-leptonic tW signal events. Most weights have similar distributions which is quite close to one. However, the weight associated with the 14th parameter has a large range, see figure 17.

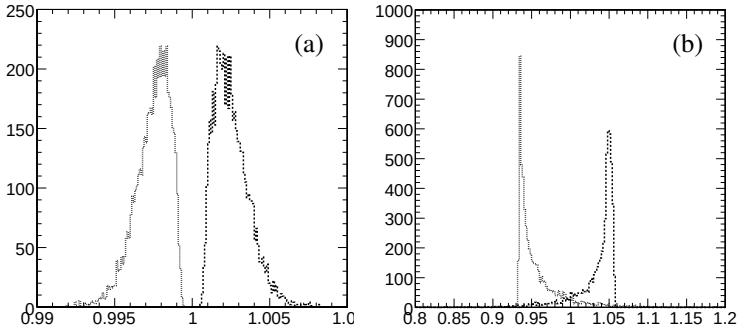

Figure 17: Distribution of 2 pairs of PDF weights w_1 (a) and w_{14} (b) in the Monte Carlo samples. Dashed histogram: 1σ upward, dotted histogram: 1σ downward.

We use FAMOS to propagate the weights to the reconstructed Monte Carlo sample to estimate the systematic uncertainties due to uncertainties in the parton distribution functions. Figure 18 illustrates the propagation of the weights through the different analysis levels, first as generated by CMKIN_6_1_0, then after detector simulation by FAMOS and finally after all selections are applied. As examples, the effects of the weights on a the top mass

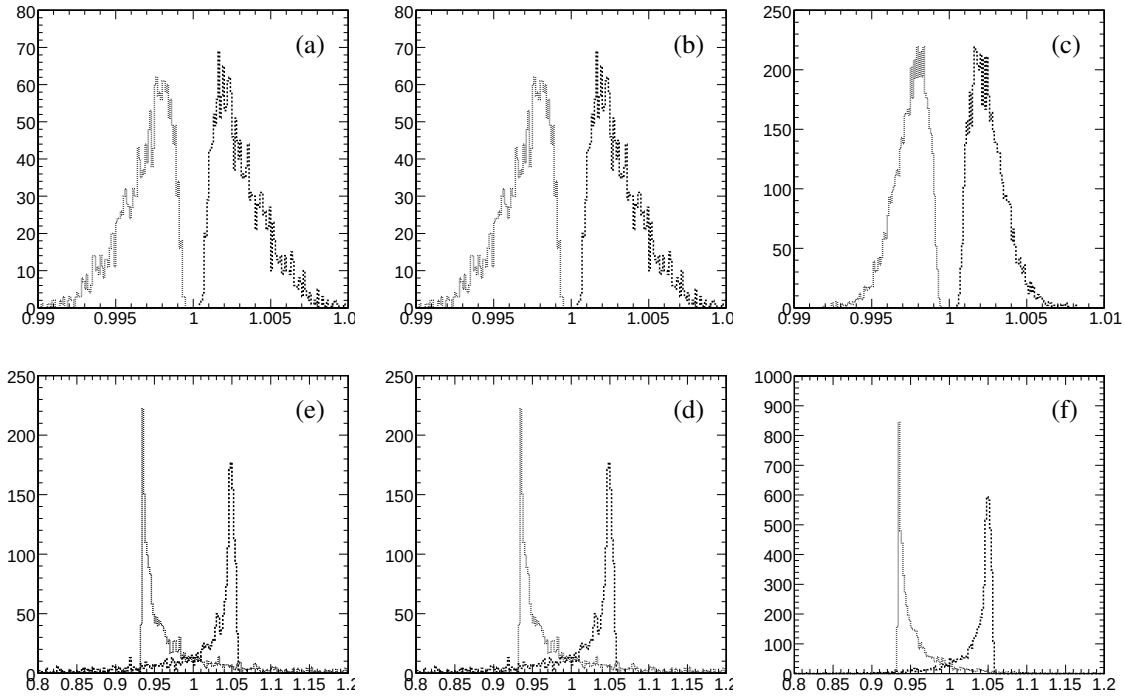

Figure 18: Distribution of the first (top) and 14^{th} (bottom) weight pairs after generation with CMKIN (left), detector simulation with FAMOS (middle) and after all selection criteria (right). Most weights behave like w_1, while w_{14} is the weight with largest deviations from 1. Dashed lines are w_i^+ and dotted lines are w_i^-.

and the transverse momentum of the top are illustrated in figure 19 for signal events in the signal region. For most weights the change in the distributions is negligible (top), however for the most sensitive weight ($w_{14}^{\pm}$) a deviation from the center value expectation is clearly visible.

With 40 weights recorded in every event, the PDF uncertainty of the cross section can be estimated with the following procedure:

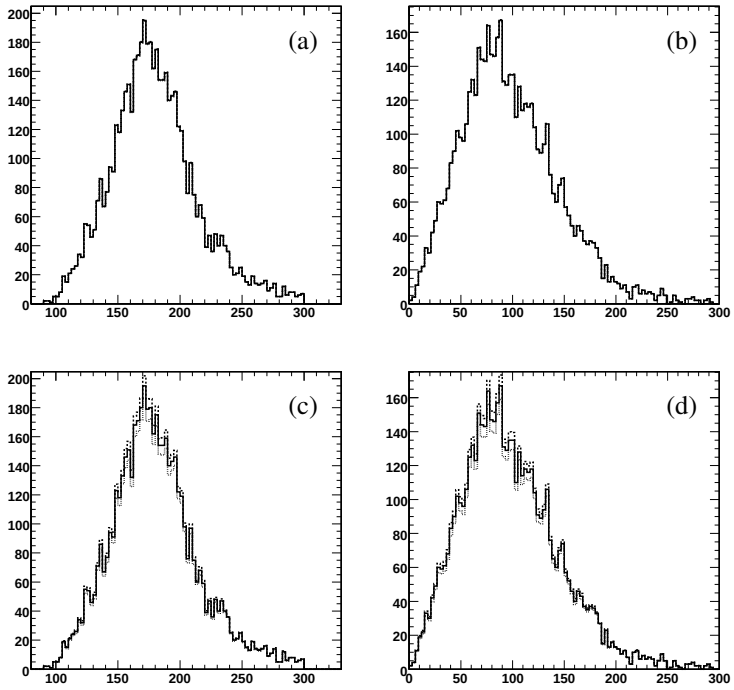

Figure 19: Distribution of the top mass (left) and the transverse momentum of the reconstructed top quark (right) for the first (top) and fourteenth (bottom) weight pairs. Solid lines are for the center value ($w_i = 1$), dashed lines are w_i^+ and dotted lines are w_i^-. Most weights behave like w_1, while w_{14} is the weight with largest deviations from one.

1. Apply all the analysis cuts on all events of the sample to produce a "selected sample", and keep the weights of every event.
2. Obtain a nominal efficiency $\epsilon = N(\text{selected sample})/N(\text{full sample})$.
3. Choose a weight pair to use, e.g., $w_i^{\pm}$, Calculate the efficiencies ϵ^+ and ϵ^-:
$$\epsilon_i^+ = \frac{\sum_{\text{selected sample}} w_i^+}{\sum_{\text{full sample}} w_i^+}, \quad \epsilon_i^- = \frac{\sum_{\text{selected sample}} w_i^-}{\sum_{\text{full sample}} w_i^-}$$
4. Calculate the shifted cross section σ_i^+ and σ_i^- with the shifted efficiency.
5. Repeat for all parameter pairs (i = 1 ... 20).
6. Calculate the total PDF systematics on cross section Δ_σ by addition in quadrature since those 20 parameters have no correlations among them. The summation is done by adding all the larger positive shifts together for Δ_σ^+ and likewise for negative shifts:
$$\begin{aligned} \Delta_\sigma^+ &= \sum_{i=1\ldots20}^{\oplus} \max(\sigma_i^+ - \sigma_0, \sigma_i^- - \sigma_0, 0), \\ \Delta_\sigma^- &= \sum_{i=1\ldots20}^{\oplus} \max(\sigma_0 - \sigma_i^+, \sigma_0 - \sigma_i^-, 0). \end{aligned}$$

To take into account the backgrounds for which PDF weights are not available in the Monte Carlo sample, we assume that the relative uncertainties in the unweighted samples are the same as the weighted samples and scale up the systematic uncertainties obtained from weighted samples by a factor
$$\frac{\sum_{\text{all samples}}^{\oplus} \text{Yield}}{\sum_{\text{weighted samples}}^{\oplus} \text{Yield}}$$

which is found by standard error propagation.

The systematic uncertainty for the semi-leptonic channel is found to be 1.6%. For the di-leptonic channel the addition in quadrature is replaced by a linear sum to be conservative and the result is $+4.4\%/-6.0\%$.

8.6 Amount of pile-up events

The pile-up uncertainty can be regarded as having two components: on the amount of pile-up, and on the modeling of the pile-up itself. In this analysis only the first kind of uncertainty has been estimated.

The average number of pile-up events is determined by the instantaneous luminosity and total cross section of proton-proton collisions. The instantaneous luminosity may fluctuate by a factor of two during an LHC fill, and the total cross section used in Monte Carlo generators (e.g., Pythia) may vary from 55.2 mb to 101.3 mb depending on the parameters used [25], another factor of 2.

To accommodate the factors, Monte Carlo samples generated with no pile-ups, nominal pile-ups and double pile-ups are used for the estimation of the systematic uncertainties due to pile-ups. The change in cross section between the no pile-ups sample and the double pile-ups sample indicates a reference of how sensitive the analysis is to pile-ups. However, quoting such a change as the systematic uncertainty is too conservative. We take a 30% difference between normal pileup and no pileup as an estimate of the systematic uncertainty, as was done in the di-leptonic $\mathrm{t\bar{t}}$ studies.

Di-leptonic channel The Monte Carlo samples used are di-leptonic tW (46k events) and $\mathrm{t\bar{t}}$ (190k events). One more sample with nominal pile-up is used as a reference sample. The analysis is found to be rather sensitive to the pileup, as the relative shift of the "measured" cross section is $+20.4\%$ for no pileup, and -16.2% for double pileup, while is the difference between the check sample and the reference sample 4.6% (which has purely statistical origin). We quote 6.1% as the systematic uncertainty for the di-leptonic channel.

Semi-leptonic channel The same method is applied for the semi-leptonic channel using TopReX + FAMOS samples with the following statistics: zero pile-up: 142k tW + 126k $\mathrm{t\bar{t}}$, double pile-up: 172k tW + 160k $\mathrm{t\bar{t}}$. The extracted cross section varies by $+35\%$ for no pileup and -63% for double pile-up so a systematic uncertainty of 10.3% is obtained.

8.7 Monte Carlo statistics

The systematic uncertainty due to the limited statistics of the Monte Carlo samples is estimated with the change in cross sections from Poisson fluctuation of the Monte Carlo events that survive all cuts. The result is 15.2% for the semi-leptonic channel and 9.9% for the di-leptonic channel.

8.8 Total systematic uncertainty

The total systematic uncertainty is obtained by addition in quadrature, assuming that the various uncertainties are uncorrelated. The results for both channels are shown in table 11.

9 Significance

In this section we describe the method used to estimate the uncertainty on the expected background yield, the estimators used to calculate the significance, and finally the significance estimated. The selection cuts of the analysis were not optimized toward maximum significance, so a higher significance may still be possible.

9.1 Significance estimators

Significance estimators can be based on either the number of events or on likelihoods. In the tW analysis we use the number of events approach because there are no reliable and discriminative physical quantities to construct a probability density function to be used in likelihoods.

Table 11: Summary of uncertainties of cross section measurement for 10 fb^{-1} of integrated luminosity.

Source	**Uncertainty**	$\Delta\sigma/\sigma$ **(di-lept.)**	$\Delta\sigma/\sigma$ **(semi-lept.)**
Statistical uncertainty	—	8.8%	7.5%
Integrated luminosity	5%	5.4%	7.8%
$\mathrm{t\bar{t}}$ cross-section	9%	*negligible*	*negligible*
t channel single top cross-section	5%	*negligible*	0.8%
W+jets cross-section	10%	*N/A*	3.1%
WW+jets cross-section	10%	1%	*N/A*
Jet energy scale	5% (20 GeV) 2.5% (50 GeV)	19.7%	9.4%
b tagging efficiency	4% (barrel) 5% (endcap)	8.7%	3.6%
PDF	1σ	$+4.4\%/-6.0\%$	1.6%
Pileup	30%×(no PU − 1xPU)	6.1%	10.3%
Monte Carlo statistics	—	9.9%	15.2%
Total systematic uncertainty		$\pm$23.9%(syst.) $\pm$9.9%(MC stat.)	$\pm$16.8%(syst.) $\pm$15.2%(MC stat.)

The results from the ratio method, equation (4), are used in the significance calculation. In addition, the uncertainty on the background expectation, Δ_B, is taken into account. In the following estimators S, B and Δ_B are all the expected values for 10 fb^{-1} of data. There are several significance estimators [26]:

$$
\begin{aligned}
S_{c1} &= \frac{S}{\sqrt{B+\Delta_B^2}}; \\
S_{c12} &= 2\frac{\sqrt{B}}{\sqrt{B+\Delta_B^2}}\left(\sqrt{S+B}-\sqrt{B}\right); \\
S_{cP} &: \int_{-\infty}^{\infty}\sum_{N=S+B}^{\infty} P(N;\mu)\,G(\mu;B,\Delta_B)\,d\mu = \int_{S_{cP}}^{\infty} G(x;1,0)\,dx. \qquad (5)
\end{aligned}
$$

In equation (5) the $P(N;\mu)$ is the Poisson probability distribution function with mean value μ, and $G(x;\bar{x},\sigma)$ is the Gaussian probability distribution with mean value $\bar{x}$ and standard deviation σ, i.e.,

$$
\begin{aligned}
P(N;\mu) &\equiv \frac{\mu^N}{N!}e^{-\mu}, \\
G(x;\bar{x},\sigma) &\equiv \frac{1}{\sqrt{2\pi}\sigma}\exp(-\frac{(x-\bar{x})^2}{2\sigma^2}).
\end{aligned}
$$

It is recommended [26] that S_{cP} should be used for counting experiments.

9.2 Estimation of Δ_B

The uncertainty of the background yield, Δ_B, is a necessary component in calculating the significances. The background yield uncertainty Δ_B obtained for the ratio method, as described in section 8, is used for the significance estimation. The systematic uncertainty of the background yield for every source is listed in table 12.

We should not take the uncertainty due to Monte Carlo statistics into account if we want to find the "expected" significance with 10 fb^{-1} of data because with such a sample the efficiencies would be estimated with a much larger real data sample. Another reason is that the Δ_B in significance estimators are supposed to be non-stochastic in origin. Nevertheless, we add them in quadrature into the total Δ_B to be conservative. The total Δ_B is then 9.6% and $+3.8\%/-4.6\%$ for di-leptonic and semi-leptonic channels, respectively.

9.3 Calculation of the significance

Basically all significance calculation uses a symmetric Δ_B. However, the asymmetric Δ_B of semi-leptonic channel can be accommodated in the S_{cP} estimator by changing the Gaussian distribution function in equation (5) to a

Table 12: Summary of uncertainties of the background yield for 10 fb^{-1} of integrated luminosity.

Source	**Uncertainty**	Δ_B/B **(di-lept.)**	Δ_B/B **(semi-lept.)**
Statistical uncertainty	—	3.6%	0.63%
Integrated luminosity	5%	2.2%	2.1%
t channel single top cross-section	5%	—	0.16%
W+jets cross-section	10%	—	0.59%
WW+jets cross-section	10%	0.4%	—
Jet energy scale	5% (20 GeV) 2.5% (50 GeV)	7.1%	+1.3%/−2.1%
b tagging efficiency	4% (barrel) 5% (endcap)	+3.2%/−3.6%	+0.68%/−2.2%
PDF	1σ	+3.0%/−2.2%	+0.4%/−0.5%
Pileup	30%	2.3%	1.7%
Total systematic uncertainty (Excluding MC statistics)		±8.9%	+2.3%/−3.4%
Monte Carlo statistics	—	3.6%	2.7%
Total systematic uncertainty		±9.6%	+3.6%/−4.4%

bifurcated Gaussian distribution function like

$$\sum_{N=S+B}^{\infty} P(N;\mu)\, G_B(\mu; B, \sigma_L, \sigma_R) = \int_{S_{cP}}^{\infty} G(x;1,0)dx \tag{6}$$

where the bifurcated Gaussian function $G_B(x;\bar{x},\sigma_L,\sigma_R)$ is defined as

$$G_B(x;\bar{x},\sigma_L,\sigma_R) \equiv \begin{cases} \frac{2}{\sqrt{2\pi}(\sigma_L+\sigma_R)}\ \exp(-\frac{1}{2}\frac{(x-\bar{x})^2}{\sigma_L^2}), & x \le \bar{x}; \\ \frac{2}{\sqrt{2\pi}(\sigma_L+\sigma_R)}\ \exp(-\frac{1}{2}\frac{(x-\bar{x})^2}{\sigma_R^2}), & x \ge \bar{x}. \end{cases}$$

We compare the significance calculated with different estimators listed in table 13, where a symmetric Δ_B is used for estimators that don't support asymmetric Δ_B.

Table 13: Comparison of significances expected for 10 fb^{-1} of integrated luminosity.

Channel	Δ_B	S_{c1}	S_{c12}	S_{cP} **Symmetric**	S_{cP} **Asymmetric**
Monte Carlo statistics included in Δ_B					
Di-leptonic	±9.6%	3.8	3.6	3.9	—
Semi-leptonic	±4.4% or $^{+3.6\%}_{-4.4\%}$	4.1	3.9	4.1	4.9
Combined				5.1	
Monte Carlo statistics not included in Δ_B					
Di-leptonic	±8.9%	4.1	3.9	4.2	—
Semi-leptonic	±3.4% or $^{+2.3\%}_{-3.4\%}$	5.1	4.9	5.1	7.0
Combined				6.4	

The significance with symmetric Δ_B is consistent among the estimators used. To be conservative, we take the S_{cP} with symmetric Δ_B as our final significance: 4.2 for the di-leptonic channel and 5.1 for the semi-leptonic channel. Combining the two channels gives a total significance of 6.4.

10 Conclusions

The W-associated production of single top quarks is studied for the CMS detector for the first time. The magnification of uncertainties from luminosity, theoretical calculation and jet energy scales due to the large $\mathrm{B/S}$ ratio is a severe challenge. We have developed a ratio method with a signal region and a high purity $\mathrm{t\bar{t}}$ background control region to eliminate the dominant $\mathrm{t\bar{t}}$ cross section uncertainty from the estimation of the tW cross section. With the ratio method, we are able to reduce the systematic uncertainties from unacceptably large values, such as 60%

from the $\mathrm{t\bar{t}}$ cross section alone, to a more acceptable one. It has been found that the expected uncertainties on the cross section measurement and significance with 10 fb^{-1} of integrated luminosity are:

$$\begin{aligned}
\tfrac{\Delta\sigma}{\sigma} \text{ (di-leptonic channel)} &= \pm 8.8\%\text{(stat.)}\pm 23.9\%\text{(syst.)}\pm 9.9\%\text{(MC stat.)}, \\
\tfrac{\Delta\sigma}{\sigma} \text{ (semi-leptonic channel)} &= \pm 7.4\%\text{(stat.)}\pm 17.7\%\text{(syst.)}\pm 15.2\%\text{(MC stat.)}, \\
S_{cP} \text{ (di-leptonic channel)} &= 4.2, \\
S_{cP} \text{ (semi-leptonic channel)} &= 5.1, \\
S_{cP} \text{ (two channels combined)} &= 6.4.
\end{aligned}$$

The uncertainties remain too large to be competitive in a direct measurement of $|\mathrm{V_{tb}}|$, and the sensitivity to $|\mathrm{V_{tb}}|$ of the tW process with the ratio method needs to be examined.

There are many sources of systematic uncertainties, and we believe that the most important ones have been addressed in this work. Other sources like minimum bias and underlying events, parameters and scale of hard process, QCD radiations, fragmentations and decays are believed not to be significant.

Acknowledgments

We would like to thank Sergey Slabospitsky, Joachim Mnich, Kati Lassila-Perini and Patrick Janot for their comments and suggestions, Maria Spiropulu, Philip Olbrechts, Markus Duda, Daniel Francois Teyssier and Monika Grothe for their prompt response in referring Monte Carlo samples to us, and Fu-Ming Tsai for his support of computer cluster.

References

[1] Q.-H. Cao and C. P. Yuan, "Single top quark production and decay at next-to-leading order in hadron collisions," *Phys. Rev.* **D71** (2005) 054022, arXiv:hep-ph/0408180.

[2] **CDF** Collaboration, A. A. Affolder et al., "First measurement of the ratio B(t→Wb)/B(t→Wq) and associated limit on the Cabibbo-Kobayashi-Maskawa element $|V_{tb}|$," *Phys. Rev. Lett.* **86** (2001) 3233–3238, arXiv:hep-ex/0012029.

[3] J. Swain and L. Taylor, "First determination of the quark mixing matrix element V_{tb} from electroweak corrections to Z decays," *Phys. Rev.* **D58** (1998) 093006, arXiv:hep-ph/9712420.

[4] Z. Sullivan, "Understanding single-top-quark production and jets at hadron colliders," *Phys. Rev.* **D70** (2004) 114012, arXiv:hep-ph/0408049.

[5] J. Campbell and F. Tramontano, "Next-to-leading order corrections to Wt production and decay," *Nucl. Phys.* **B726** (2005) 109–130, arXiv:hep-ph/0506289.

[6] S. Zhu, "Next-to-leading order QCD corrections to bg→ $\mathrm{tW^-}$ at the CERN Large Hadron Collider," *Phys. Lett.* **B 524** (2002) 283–288.

[7] A. Belyaev and E. Boos, "Single top quark tW+X production at the CERN LHC: A closer look," *Phys. Rev.* **D63** (2001) 034012, arXiv:hep-ph/0003260.

[8] T. M. P. Tait, "$\mathrm{tW^-}$ mode of single top quark production," *Phys. Rev.* **D61** (2000) 034001, arXiv:hep-ph/9909352.

[9] **ATLAS** Collaboration, D. O'Neil, B. Gonzalez-Pineiro, and M. Lefebvre, "Prospects for measuring V_{tb} via s-channel single top at ATLAS," *J. Phys.* **G28** (2002) 2657–2667.

[10] S. R. Slabospitsky and L. Sonnenschein, "TopReX generator (version 3.25): Short manual," *Comput. Phys. Commun.* **148** (2002) 87–102, arXiv:hep-ph/0201292.

[11] T. Sjostrand, L. Lonnblad, S. Mrenna, and P. Skands, "PYTHIA 6.3: Physics and manual," arXiv:hep-ph/0308153.

[12] M. L. Mangano, M. Moretti, F. Piccinini, R. Pittau, and A. D. Polosa, "ALPGEN, a generator for hard multiparton processes in hadronic collisions," *JHEP* **07** (2003) 001, arXiv:hep-ph/0206293.

[13] **CMS** Collaboration, D. Acosta et al., "CMS Physics TDR Volume 1, Section 2.6: Fast simulation," *CERN/LHCC* **2006-001** (2006) 55.

[14] **CMS** Collaboration, D. Acosta et al., "CMS Physics TDR Volume 1, Section 2.7: Event selection and reconstruction," *CERN/LHCC* **2006-001** (2006) 65.

[15] **CMS Trigger and Data Acquisition Group** Collaboration, W. Adam et al., "The CMS high level trigger," *submitted to European Physical Journal* **C** (2005) arXiv:hep-ex/0512077.

[16] G. Davatz, M. Dittmar, and A.-S. Giolo-Nicollerat, "Standard Model Higgs Discovery Potential of CMS in H$\rightarrow$ WW$\rightarrow \ell\nu\ell\nu$ Channel," *CMS Note* **2006-047** (2006).

[17] **CMS** Collaboration, D. Acosta et al., "CMS Physics TDR Volume 1, Section 11.2.1: Iterative cone," *CERN/LHCC* **2006-001** (2006) 407.

[18] S. Lowette, J. D'Hondt, and J. Heyninck, "Offline Calibration of b-Jet Identification Efficiencies," *CMS Note* **2006-013** (2006).

[19] **CMS** Collaboration, D. Acosta et al., "CMS Physics TDR Volume 1, Section 12.2: b-tagging tools," *CERN/LHCC* **2006-001** (2006) 461.

[20] R. A. Fisher, "The use of multiple measurements in taxonomic problems," *Annuals of Eugenics* **7** (1936) 179–188.

[21] **CMS** Collaboration, D. Acosta et al., "CMS Physics TDR Volume 1, Section 11.7: Association of jets with the signal vertex," *CERN/LHCC* **2006-001** (2006) 431.

[22] **CMS** Collaboration, D. Acosta et al., "CMS Physics TDR Volume 1, Section 8.5: Sources of systematic effects," *CERN/LHCC* **2006-001** (2006) 229.

[23] **CMS** Collaboration, D. Acosta et al., "CMS Physics TDR Volume 1, Section 11.6.3: γ+jet events," *CERN/LHCC* **2006-001** (2006) 423.

[24] M. A. Dobbs et al., "Les Houches guidebook to Monte Carlo generators for hadron collider physics," arXiv:hep-ph/0403045.

[25] P. Bartalini, R. Chierici, and A. De Roeck, "Guidelines for the Estimation of Theoretical Uncertainties at the LHC," *CMS Note* **2005-013** (2005).

[26] M. Davids, "Uncertainties and Discovery Potential in Planned Experiments," *CMS CR* **2002-005** (2002).